# Slowly migrating fracture swarms in an actively serpentinizing borehole

**John M. Aiken[1,2], Fabian Barras[1], François Renard[1,3], Greg Hirth[4], Peter B. Kelemen[5], Robert A. Sohn[6]**

[1]Njord Centre, Departments of Geosciences and Physics, University of Oslo, PO BOX 1048, Blindern, 0316 Oslo, Norway
[2]Expert Analytics, Oslo, Norway
[3]Univ. Grenoble Alpes, Grenoble INP, Univ. Savoie Mont Blanc, CNRS, IRD, Univ. Gustave Eiffel, ISTerre, 1381 rue de la Piscine, 38000 Grenoble, France
[4]Department of Earth, Environmental, and Planetary Sciences, Brown University, Providence, RI, USA
[5]Lamont-Doherty Earth Observatory, Columbia University, Palisades, NY, USA
[6]Department of Geology and Geophysics, Woods Hole Oceanographic Institution, 266 Woods Hole Rd., Woods Hole, MA 02543, USA

**Key Points:**

- Hydrophones have detected slow propagating fracture swarms in a borehole in Oman peridotites.
- Tensile fracture swarms occur during a period of higher than normal pore pressures due to rain.
- Injecting carbon dioxide into peridotite may induce slow fracturing and enhance permeability.

---

Corresponding author: John M. Aiken, `johnm.aiken@gmail.com`

**Abstract**

Peridotite rocks are primary targets for engineered geological carbon sequestration efforts because the carbon in $CO_2$-bearing fluids is transferred to the rock in the form of carbonate minerals during alteration reactions. Sequestration efforts must necessarily open fractures in the rocks surrounding a pumped borehole, but the current understanding of fracture growth during serpentinization of peridotite is limited to theoretical models and laboratory experiments on small samples. We deployed hydrophone arrays in peridotite boreholes established by the Oman Drilling Program and detected downward migrating earthquake swarms that represent the first field observations of active fracture growth in a serpentinizing rock. More than two years after the boreholes were established, we detected four, downward migrating tensile fracture swarms during an interval of elevated pore pressure following large rain events. All of the swarms occurred within a partially-confined section of the local aquifer, beginning at a depth of ∼170 m and migrating to the bottom of the 400 m-deep hole at average rates of ∼6-20 cm.s$^{-1}$.We demonstrate that pore fluid processes can explain both the triggering of the tensile fracture swarms and their slow migration rates. Our results indicate that crack tip stresses in the fractures propagating away from the borehole maintained near-critical levels over time such that relatively small increases in fluid pressure triggered tensile fracturing episodes, suggesting that pumping efforts for carbon sequestration should be able to induce fracture opening and propagation.

## Plain Language Summary

Scientists are exploring ways to store carbon dioxide underground by pumping carbonated water into deep holes drilled in special rocks called peridotites. These rocks can react with the water and carbon dioxide to form new minerals, which locks away the carbon safely. This study monitored two boreholes in Oman and found that, even years after drilling, new fractures formed in the rock during times of high water pressure and chemical changes. The fractures grew slowly, likely because water was moving into the cracks as they formed. These findings show that chemical reactions between water, carbon dioxide, and rock can help create new pathways for fluids, which is important for improving carbon storage in the future.

## 1 Introduction

Pumping carbonated water into boreholes drilled into mafic rocks, such as basalts or peridotites, is an emergent technology of engineered geological carbon sequestration (Gislason and Oelkers 2014). In peridotites, the water-rock reactions transfer $CO_2$ from the water to the rock via mineral carbonation, and the effectiveness of this approach depends on the ability to stimulate fracture growth to open pore space and expose fluids to fresh rock. Peridotite rocks have low bulk permeability but contain complex multi-directional fracture networks that support fluid flow and ongoing alteration (Iyer et al. 2008; Kelemen, Leong, et al. 2021; Aiken, Dufornet, et al. 2025). The serpentinization and carbonation water-rock reactions increase the solid volume of the rock and exert a force of crystallization, and it has been hypothesized that the resulting stress perturbation facilitates the opening of new fractures, which in turn sustains ongoing alteration (Kelemen and Matter 2008; Jamtveit, Putnis, and Malthe-Sørenssen 2009; Kelemen, Matter, Streit, et al. 2011; Kelemen and Hirth 2012; Plümper et al. 2012; Okamoto and Shimizu 2015; Malvoisin, Brantut, and Kaczmarek 2017; Renard 2021). This *reaction-driven fracturing* hypothesis predicts that crack tip stresses in active alteration zones will continually increase and reach critical levels for failure, which, if true, should facilitate the opening of new fracture surface area for carbon sequestration efforts.

The Multi-Borehole Observatory (MBO) of the Oman Drilling Program (OmanDP) is located in Wadi Lawayni, a dry wash that cuts through mantle rocks of the Samail ophiolite in Oman (Figure 1). The MBO established four boreholes, providing a unique opportunity to study near-surface peridotite alteration and the chemosynthetic biosphere that feeds on the reaction byproducts ((Templeton, Ellison, Glombitza, et al. 2021; Hatakeyama et al. 2021; Kelemen, Leong, et al. 2021; Callegari et al. 2022; Sohn and Matter 2023)), and, ultimately, to begin to test the reaction-driven fracturing hypothesis. Here we used downhole hydrophone arrays to monitor fracturing on the walls of two boreholes, spaced 100 m apart, for nine months.

The introduction of a circular opening into rock generates stress concentrations around the borehole walls that can lead to fracturing and deformation (Jaeger, Cook, and Zimmerman 2009). The nature of the deformation depends on the magnitudes of the local principal stresses, the pore fluid pressure in the surrounding rock matrix, and the tensile strength of the wall rocks (e.g. (Zoback et al. 1985; Zheng, Kemeny, and Cook 1989)). It is typically assumed that borehole deformation in response to drilling-induced stresses occurs within the first hours to days following the creation of a borehole (Moore et al. 2011) and that further deformation requires an additional mechanism to either weaken the rock or increase crack tip stresses (Zoback et al. 1985). In a peridotite borehole it is thus also necessary to consider the effect of alteration. Theoretical models and laboratory experiments developed and conducted to understand fracturing during peridotite alteration indicate that alteration products can increase crack tip stresses and promote fracture growth through a process commonly known as reaction-driven cracking (e.g., Kelemen and Matter 2008; Jamtveit, Putnis, and Malthe-Sørenssen 2009; Kelemen, Matter, Streit, et al. 2011; Kelemen, Leong, et al. 2021). None of these models or experiments, however, consider the growth of drilling-induced fractures, and, critically, there are no field observations of active fracture growth in peridotite boreholes.

Our study addresses this knowledge gap by providing hydrophone array observations of downward migrating fracture swarms in hole BA1A of the MBO. Over the course of a nine month deployment we observed four such swarms, all of which occurred during a period of elevated pore pressure in the formation following large rain events. The depth interval of fracture propagation closely corresponds to the interval of active serpentinization indicated by the borehole fluid compositions (Kelemen, Leong, et al. 2021), and the fractures propagate at low rates commonly associated with slow earthquakes (Ide and Beroza 2023). Our results thus provide valuable insight into fracture growth in peridotite boreholes with relevance to geological carbon sequestration efforts and a unique perspective on the role of pore fluids in modulating fracture propagation rates.

## 2 Methods

### 2.1 Site Description

The MBO consists of four, ∼400 m deep boreholes within a ∼100 x 100 $m^2$ area, three of which were drilled with 15.2 cm diameter (BA1A, BA1C - collapsed, BA1D), and one of which was cored with a 9.6 cm diameter (BA1B) (Kelemen, Matter, Teagle, et al. 2020). The lithological structure of the site is constrained by downhole observations and core sample analyses, and overall consists of dunites to a depth of ∼160 m that are underlain by less depleted harzburgites (Kelemen, Leong, et al. 2021). The near-surface zone down to ∼50 m is extensively fractured and contains cross-cutting carbonate and serpentinite veins. Below ∼50 m the degree of fracturing decreases and carbonate alteration is no longer observed. Veins and fractures are sparse below ∼160 m in the harzburgites, with porosities $\leq \sim 1\%$ (Katayama et al. 2020). The complex fracturing and alteration history of the rocks is due to a combination of the mid-ocean ridge process during formation and more recent obduction and subaerial weathering. Downhole fluid pH and oxygen fugacity measurements at the BA site demonstrate that low-temperature serpentinization is ongoing at depths below 150 m (Kelemen, Leong, et al. 2021) and the observation of bubble swarms episodically discharging into hole BA1B (Aiken, Sohn, et

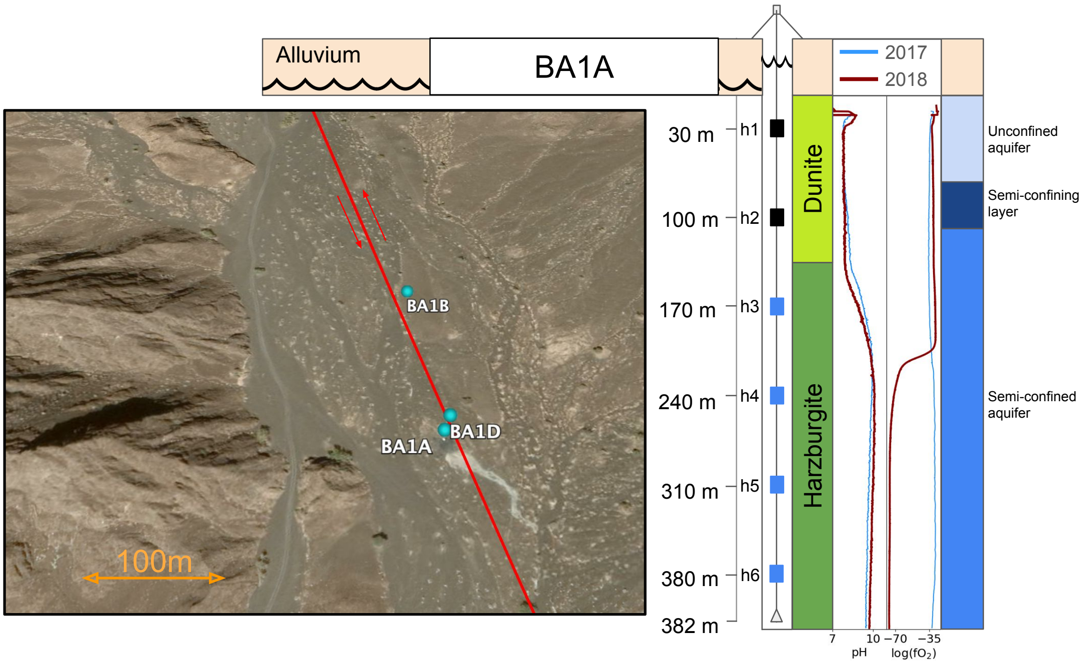


**Figure 1.** Location of the OmanDP Multi-Borehole Observatory (MBO) in a mantle section of the Samail ophiolite in Wadi Lawayni, Oman. The red line represents a left-lateral fault that transects the MBO (Callegari et al. 2022). Three boreholes (BA1A, BA1B, BA1D) were drilled in a ∼100 x 100 m area (another borehole, BA1C, not shown, collapsed during drilling). Six-element hydrophone arrays were deployed for nine months in boreholes BA1A and BA1B. The fracture swarms described here were detected by the bottom four phones (h3 - h6, colored blue) in borehole BA1A (data from the top two phones, colored black, were corrupted by electrical noise). The increase in pH and drop in oxygen fugacity measured one year after drilling and reported in (Kelemen, Leong, et al. 2021) are reprinted here. The primary lithological (Kelemen, Leong, et al. 2021) and hydrological (Lods et al. 2020) structure of hole BA1A are shown on the right.

al. 2022; Liu et al. In Review) indicates that free gas generated by serpentinization is present and highly mobile in the subsurface.

The hydrologic structure of the MBO site is heterogeneous but overall consists of a high-permeability near-surface zone underlain by a low-permeability aquifer (Lods et al. 2020). Flow in the near-surface zone ($\leq \sim$50 m depth), corresponding to the zone of intense fracturing in the lithological record, is focused within a network of multi-directional heterogeneities. The aquifer surrounding boreholes BA1A and BA1D is partially confined by a low permeability layer at ~100-130 m depth, which allows it to be pressurized by external loads. In contrast, pore pressure in the aquifer surrounding borehole BA1B does not respond to barometric or tidal loads, indicating that the aquifer is locally unconfined (Sohn and Matter 2023). The aquifer response to loading thus changes markedly over the ~100 m distance between boreholes BA1A and BA1B.

### 2.2 Rain and Borehole Water Level Data

We acquired water level at 15 minute intervals in borehole BA1D using a Rugged TROLL non-vented data logger from In-Situ Inc. The non-vented pressure data were corrected by subtracting contemporaneously measured atmospheric pressure data and converted to relative water level assuming a fluid density of 1000 kg.m$^{-3}$. We retrieved daily precipitation rates for the MBO catchment from the Copernicus Climate Reanalysis Data Store (Store 2017) using the catchment shape defined by the hydroBASINS data set (Lehner and Grill 2013) (Figure 6). The water levels in borehole BA1D rose rapidly by ~5 m following two large rain events in April and May 2019 and then slowly decreased until the end of the hydrophone array deployments.

### 2.3 Acoustic Data

We deployed hydrophone arrays, each consisting of six High Tech HTI-96-MIN hydrophones with a 70 m inter-element spacing, in boreholes BA1A and BA1B (Figure 1) from May 2019 to February 2020. The data were sampled at 1 kHz and recorded using a Quanterra Q330S+ data logger with a low-pass (450 Hz) anti-aliasing filter.

We detected downward-migrating event swarms in hole BA1A on four days (days 141, 188, 197, and 211) in 2019 (Figures 3, 5). We detected individual events within the high-rate swarms by extracting data windows extending from ~15 minutes before the swarm starts until ~15 minutes after it ends, high-pass filtering (50 Hz, zero-phase) the extracted records, and squaring the signal amplitude. We generated a preliminary event catalog by applying a peak finding algorithm to each processed record and associating detections across the hydrophone array. We generated arrival time estimates for each event by selecting a 0.4 second window centered on the initial detection time, calculating the Akaike Information Criterion (AIC) for each trace (Maeda 1985), and picking arrival times based on the maximum value of the AIC time-derivative (Figure 3).

The arrival time and amplitude of the short duration (~200 ms) signals across the vertical hydrophone array exhibit a systematic pattern, with the earliest arrivals having the highest amplitudes and the arrival time difference between the two hydrophones with the earliest arrivals, i.e., the "bounding phones", being between zero and ~40 ms (Figure 3). Signal amplitudes decrease with distance, up or down the array, from the bounding phones and the arrival time difference between all other adjacent hydrophone pairs is a constant value of ~40 ms, corresponding to an apparent phase velocity of ~1750 m.s$^{-1}$. This phase velocity is too slow for a body wave propagating in the rock, which has compressional velocities of ~5.6 km.s$^{-1}$ and shear velocities of ~2.9 km.s$^{-1}$ (Hatakeyama et al. 2021), but is consistent with a trapped fluid mode propagating inside the borehole from a source near the borehole wall (Schoenberg et al. 1981).

We estimated the source depth of each event based on the arrival time of the propagating phase at the bounding phones. If the arrival time is $t_i$ at the upper bounding hydrophone with depth $z_i$ and $t_j$ at the lower bounding hydrophone with depth $z_i + 70$ m, then the source depth, $z$, in meters is given by (Figure 3):

$$z = z_i + 35 - 0.5 \times dt \times v \quad (1)$$

where $dt = t_i - t_j$ and $v$ is the trapped wave propagation velocity (1750 m.s$^{-1}$).

Given the 1 kHz sampling rate of the data, the depth estimates are discretized into 0.875 m intervals. The absolute uncertainty of the depth estimates, assuming a phase arrival time uncertainty of 3 ms and a propagation velocity uncertainty of 10%, is $\sim$4 m. For about 10-15% of the events in each swarm, and primarily for small events with low signal-to-noise ratios, the automated picking algorithm generated erroneous arrival time estimates that could not be used for depth estimation, and these events were removed from the final catalog. We cannot estimate the seismic moment of the events because the amplitude of a trapped fluid mode is a function of radial position in the borehole, which is unknown for the hydrophones.

We estimated the average downward migration velocity of each swarm using a least squares method weighted by the number of events in 30-second windows to fit the equation: $\hat{d} = \beta_0 + \hat{v}t$, where $\hat{d}$ is the predicted depth, $\beta_0$ is the intercept, $\hat{v}$ is the estimated velocity, and $t$ is the time of the event. We then estimated the instantaneous rupture front velocity during each swarm using a piecewise technique averaged over 10-second intervals. After selecting an initial event for the starting point of the migration, the algorithm advances chronologically through the event catalog searching for the next deeper event and then calculating the instantaneous propagation velocity based on the difference in event depths and origin times. A threshold velocity, which was manually tuned to each swarm in the range 20-30 cm.s$^{-1}$, was used to prevent the algorithm from latching onto outliers. The process is repeated until the end of the catalog is reached and time-averaged instantaneous velocity estimates are then generated on 10-second intervals. The algorithm follows the leading edge of the rupture front and its piecewise nature allows it to follow the multiple strands observed during the day 188 swarm by starting at different times in the catalog.

All days produce broad spectrum results on spectrogram analysis of the swarms (Fig. 4). Horizontal lines at 100Hz, 200Hz, 300Hz, and 400Hz, are electrical noise from the hydrophone cables. Spectral horizontal lines visible below 100Hz correspond to resonant frequencies as reported in Liu et al. In Review.

## 3 Results and Discussion

Data records from borehole BA1A contain intense swarms of small, downward migrating rupture events that occurred during four days of the nine-month deployment (days 141, 188, 197, and 211 of the year 2019). The downward propagating nature of the events is evident in the raw vertical array data (Figure 2) and the impulsive events have typical acoustic amplitudes of $\leq$3 Pa, durations of $\sim$200 ms, and recurrence intervals of $<$ 1 s.

The individual swarms had event counts ($N_x$ = count for swarm on day of year $x$) that varied from $N_{141}$=2954 to $N_{188}$=4009 to $N_{197}$=1216 to $N_{211}$=586, with durations (hour:minute:second) of $D_{141}$=00:59:06, $D_{188}$=01:16:31, $D_{197}$=01:50:22, and $D_{211}$=00:26:21. Each swarm began near the depth horizon of hydrophone h3 ($\sim$170 m) and migrated towards the bottom of the borehole (Figure 5). The migration patterns are patchy, with discrete depth intervals of fracturing interspersed with quiet zones where no events were detected. The swarms on days 141 and 211 exhibit an essentially monotonic downward

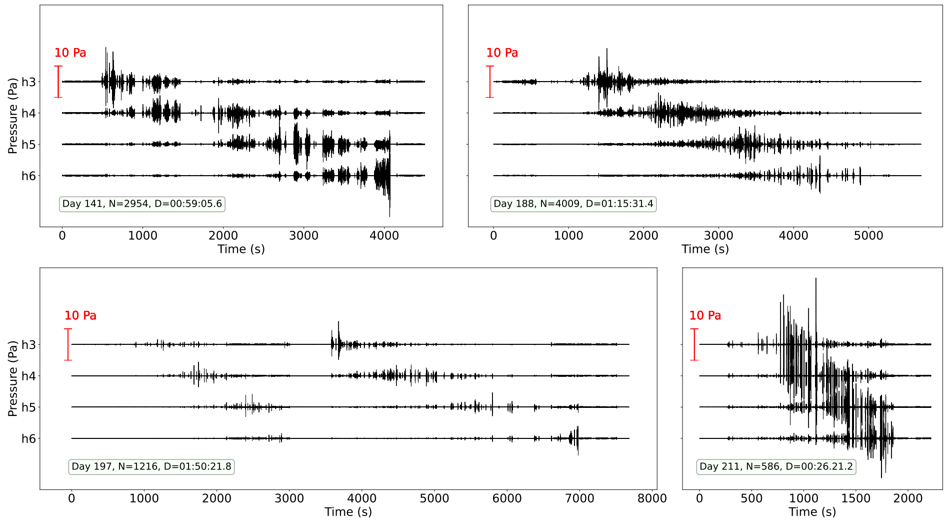


**Figure 2.** Raw hydrophone data for each event swarm, labeled by day of the year (2019). The number of detected events ($N$) and duration of the swarm ($D$) are reported in each panel.

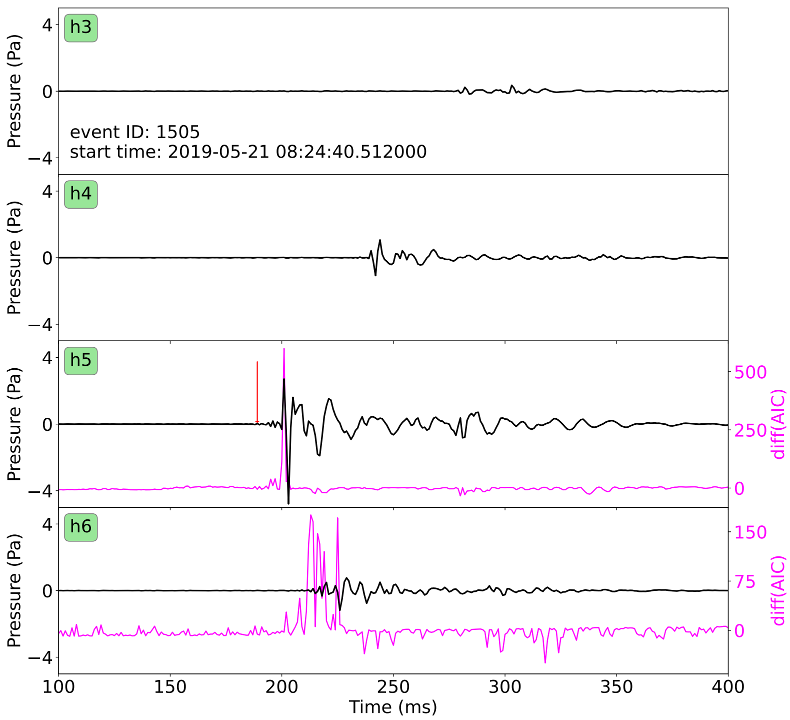


**Figure 3.** Example event waveforms recorded on hydrophones h3 to h6. Arrival time estimates are made using the AIC finite difference calculation for the two bounding hydrophones (h5 and h6 in this case).

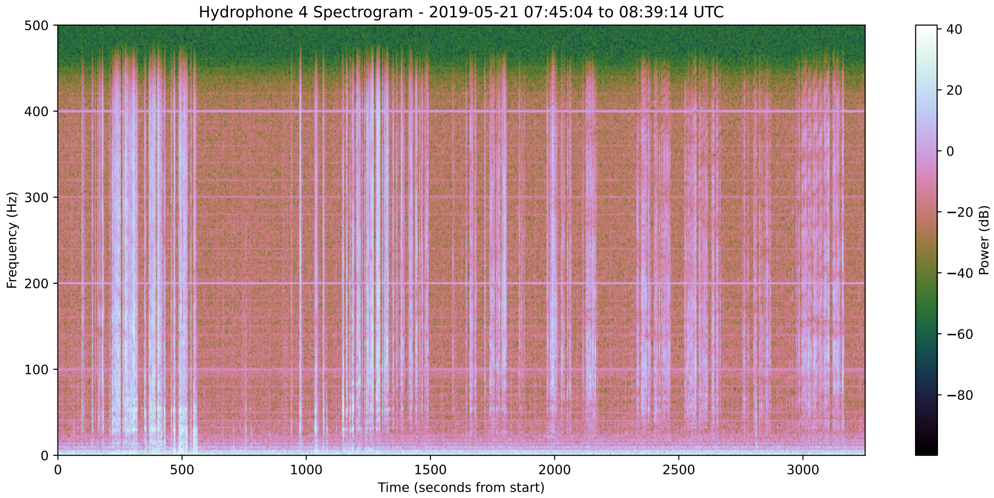


**Figure 4.** Spectrogram for the day 141 swarm on hydrophone 5.

migration but the swarms on days 188 and 197 are more complex (Figure 5). The swarm on day 188 appears to contain three distinct migration strands, indicating that multiple rupture fronts were active at the same time. The swarm on day 197 has two distinct migration episodes, with a weak, initial episode that did not reach the bottom of the borehole followed by a second, more energetic episode that reached the bottom of the hole.

All of the swarms have median migration rates of ∼6-10 cm.s$^{-1}$, with the exception of the final swarm on day 211, which had the largest events and a faster average migration rate of ∼20 cm.s$^{-1}$ (Figure 5). The instantaneous rupture front velocity estimates range from $\leq 1$ cm.s$^{-1}$ up to ∼15 cm s$^{-1}$ for all swarms except that on day 211, which had a minimum velocity of 6 cm.s$^{-1}$ and a maximum velocity of ∼30 cm.s$^{-1}$. There is no apparent correlation between depth and rupture front velocity and fracturing within a given depth interval typically continues at decreasing rates for ∼1 min after the front passes.

### 3.1 Borehole Stresses and Fracturing

The hoop stresses around a borehole are given by the Kirsch solution (Jaeger, Cook, and Zimmerman 2009):

$$\sigma_\theta = \frac{(\sigma_H + \sigma_h)}{2}(1 + \frac{a^2}{r^2}) - \frac{(\sigma_H - \sigma_h)}{2}(1 + 3\frac{a^4}{r^4}) \cos 2\theta - P(\frac{a^2}{r^2}), \tag{2}$$

where $a$ is the borehole radius, $r$ is the radial distance from the borehole axis, $\theta$ is the angle from the maximum principal stress, $P$ is the fluid pressure inside the borehole, and $\sigma_H$ and $\sigma_h$ are the local maximum and minimum principal stresses, respectively. Maximum tensile stresses are aligned with the maximum principal stress springline ($\theta \approx 0°$, 180°), and if the length of a tensile crack growing away from the hole is much less than the borehole radius (i.e., $r \approx a$), the criterion for crack growth can be approximated by:

$$3\sigma_h - \sigma_H - p - \sigma_{wr} < -T, \tag{3}$$

where $T$ corresponds to the tensile strength of the rock and $P$ in Eq. 2 has been decomposed as the sum of the fluid pressure $p$, $\sigma_H$ and $\sigma_h$ are respectively the largest and low-

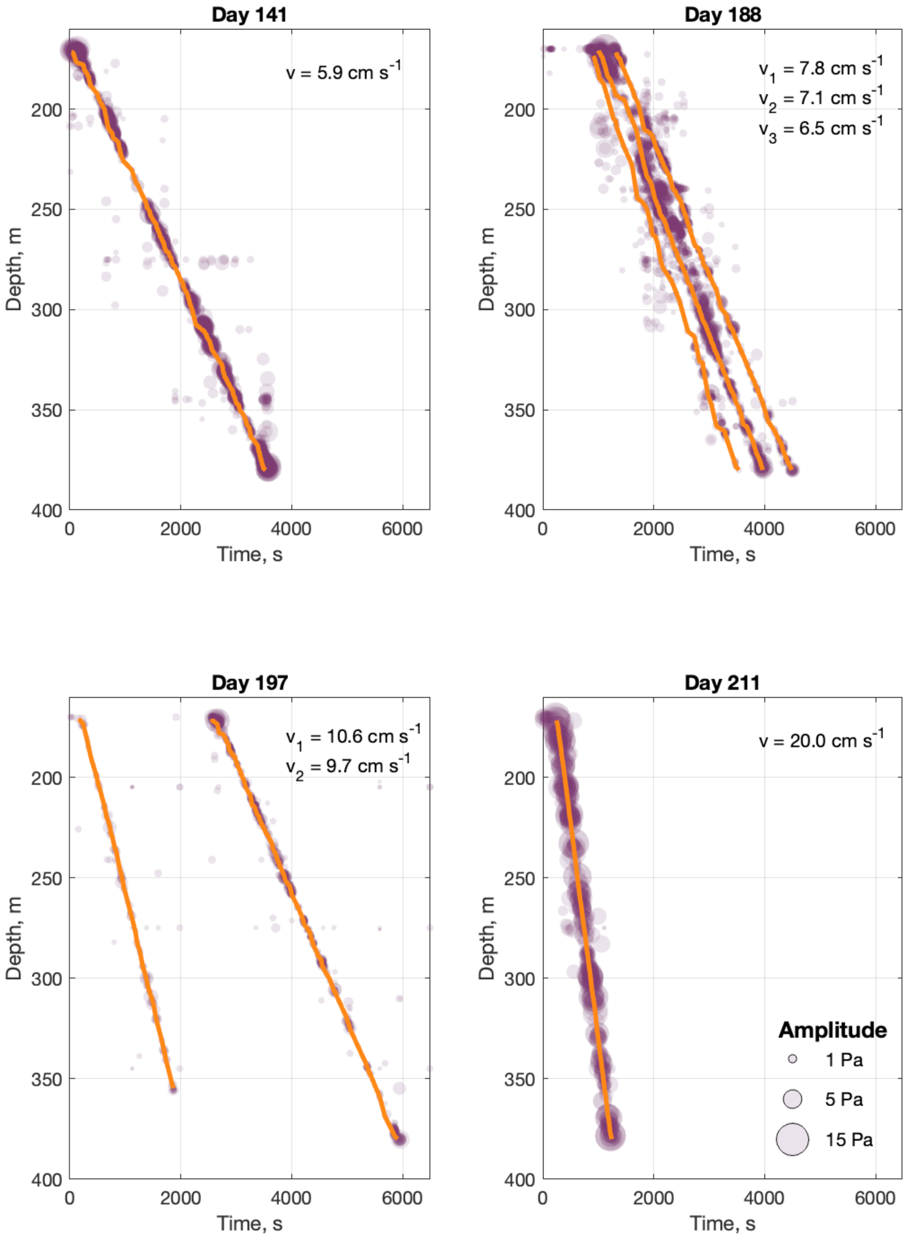


**Figure 5.** Event size and depth versus time for each swarm. Event size is shown by symbol size (see legend) and the solid orange lines indicate piecewise tracking of rupture fronts (see Section 2.3). Median values of the instantaneous rupture front velocity estimates are listed.

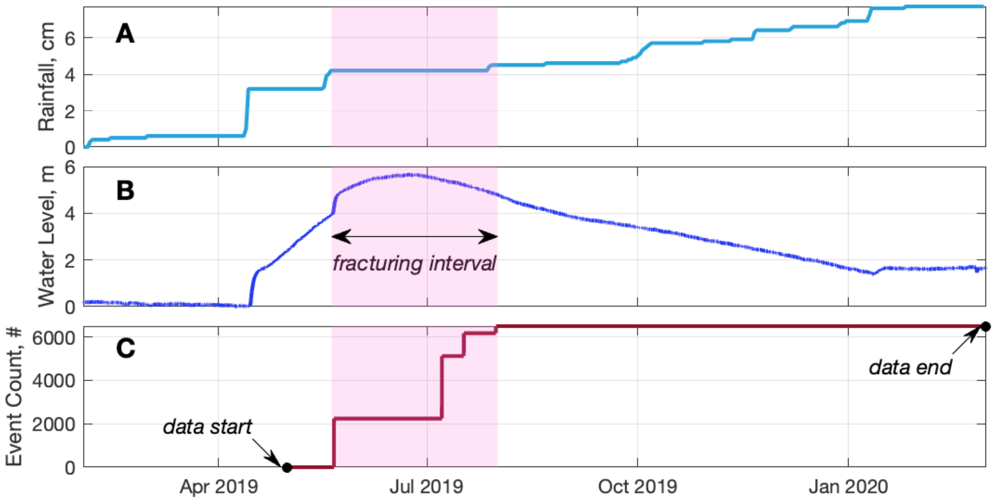


**Figure 6.** A) Cumulative daily precipitation for the MBO catchment. B) Relative water level data from borehole BA1D. C) Cumulative fracturing events count. The time interval during which the rupture swarms occurred is highlighted in the three panels.

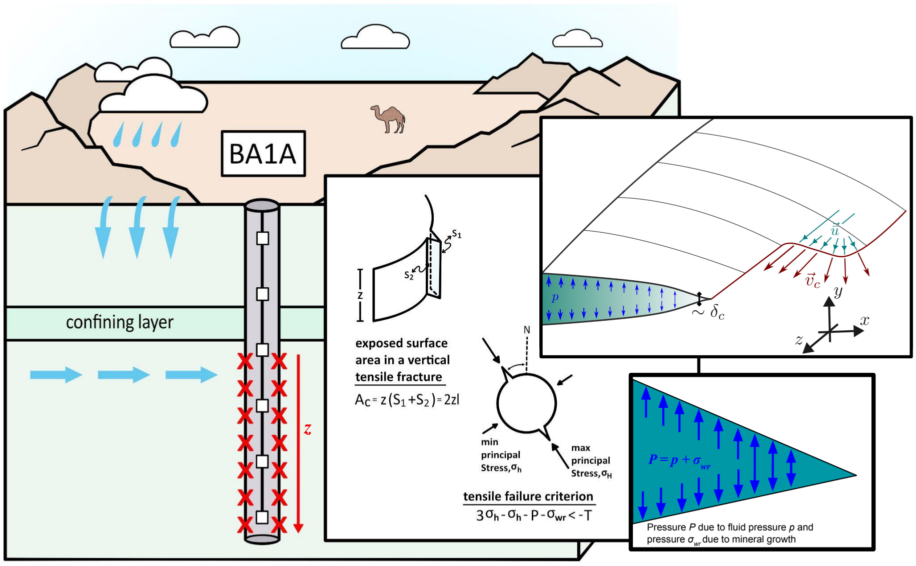


**Figure 7.** Boreholes BA1A and BA1D of the Oman Drilling Project Multi-Borehole Observatory. Drilling a borehole caused tensile fractures (inset, right) due to the relaxation of tectonic stresses. These fractures allowed fluid in the borehole (i.e., water) to infiltrate the fracture planes and over the two-year period this caused unaltered peridotites to serpentinize within the tensile fracture zone. Serpentinization of peridotite leads to a decrease in oxygen fugacity and increase in pH (Figure 1) as well a volumetric increase which causes strain ($\epsilon_s$) on the surrounding rock. Rainfalls recharge the aquifer increasing the pore-pressure due to the confinement from the low porosity layer. This pore pressure increase reached a critical limit leading to downward migrating tensile fracture swarms in borehole BA1A.

est compressive stress, and $\sigma_{wr}$ accounts for the increase in normal stress due to chemical alteration of the rock. and the pressure caused by the growth of minerals from water rock reactions on the fracture surface $\sigma_{wr}$. Drilling-induced stresses decay rapidly with distance from the borehole and the associated deformation typically occurs within the first hours to days after the borehole is established (Moore et al. 2011). Continued fracture growth more than two years later, as we observed, requires a hydraulic fracture mechanism that maintains near-critical stress levels over time.

The hydraulic fracture setup is sketched in Figure 7. The tensile fracture is caused by the elastic stress perturbation due to the borehole (Eq. 3). Fluid pressure is assumed to be hydrostatic within the fracture between swarms $p(x, z) = \rho_w g z$. A rupture event initiates at the depth of the confining layer due to a local increase in fluid pressure. During swarms, the crack grows and fluid invades the newly created fracture cavity. Following hydraulic fracture, we assume a Poiseuille fluid velocity profile such that flow is characterized by an average flow rate $\vec{\bar{u}}$ across the thin aperture $\delta$. Neglecting the contribution of inertia and fluid exchange with the host rock, lubrication flow through the fracture can be expressed as a two-components vector:

$$\vec{\bar{u}} = -\frac{\delta^2}{12\mu_w}(\nabla p - \rho_w \vec{g}). \tag{4}$$

In the radial direction $r$, flow rate is driven by the gradient in pressure created by the motion of the fracture tip and the associated fluid pressure drops. During crack growth, hydraulic fracture model and experiments typically observe a transient lag between the fronts of the invading fluid and the one of the propagating crack tip, such that fluid pressure is assumed to be vanishingly small in the near-tip region $r = a$. In the vertical direction $h$, fluid is flowing downwards driven by vertical pressure gradient plus a gravitational contribution.

Crack growth is assumed to follow the description of Linear Elastic Fracture Mechanics and arises as long as the tensile stress intensity factor at the tip exceeds the fracture toughness of the rock $K_{I,c}$. Due to the large confining stresses existing far from the borehole, the radial expansion of the crack during each event is expected to be small compared to the initial crack size, which is supported by the small amplitudes of the measured acoustic events. From the observed dynamics of the swarms, crack growth starts from the confining layer and progressively migrates downwards. Interestingly, a similar tangential crack growth is also observed at the laboratory scale in the context of fluid-driven fracture (Cochard et al. 2024). From hydraulic fracture theory, crack propagation speed is quasi-static and well approximated by the velocity of lubrication flow in the near-tip region $\vec{v}_c \approx \vec{\bar{u}}(r = a)$.

As sketched in Figure 7, the vertical flow in the freshly created fracture space is of particular interest and arises through the low-pressure, small-aperture region near the tip. Invoking these conditions, we assume that, in the near-tip cavity, the gravity term in Eq.(4) dominates the pressure gradient along the vertical direction. This assumption is further supported by the fact that crack growth arises over much larger distances along the vertical direction than along the radial direction. The vertical crack propagation speed can then be written as:

$$v_{c,z} = \frac{\delta^2}{12\mu_w}\rho_w g. \tag{5}$$

Last, we use a cohesive zone model of fracture to estimate the order of magnitude of the crack aperture in the tip region from the critical opening distance $\delta(r = a, z)/\delta_c \approx 1 - 10$. The latter is expressed as function of the fracture toughness $K_{I,c}$, the tensile strength $T$ and the elastic parameters of the host rock:

$$\delta_c = \alpha \frac{K_{I,c}^2(1-\nu)}{\mathcal{G}T}, \tag{6}$$

with $\mathcal{G}$ and $\nu$ being respectively the shear modulus and Poisson's ratio of the host rock and $\alpha$ a constant that corresponds to unity for linear cohesive law or to $\alpha = e$ for exponential cohesive law. The combination of Eqs. (5) and (6) leads to the scaling of the swarm migration speed reported in Eq. (7).

A left-lateral strike-slip fault runs through the MBO site, but geological mapping and remote sensing imagery indicate that activity on this fault ceased ∼20 Ma (Callegari et al. 2022) and there is no evidence of activity in regional earthquake catalogs or in our hydrophone array data. We thus assume that the regional principal stresses, $\sigma_H$ and $\sigma_h$, did not change on the timescale of our observations, leaving fluid pressure, $p$, and water-rock reaction induced stresses, $\sigma_{wr}$ as the time-dependent stress parameters (Eq. 3) that could trigger the observed fracture swarms. Given the short (∼10 m) distance between boreholes BA1A and BA1D, and their similar hydrological structure (Lods et al. 2020), the water level data from borehole BA1D provides a proxy for fluid pressure in borehole BA1A, demonstrating that it increased by ∼54 kPa following large rain events in April and May, 2019. The hydrophone arrays were not in place during the first rain event in April 2019, but the first swarm we observed occurred immediately after fluid pressure rose following the rain event in May 2019, and all the swarms occurred during a 70-day interval when borehole fluid pressures were maximal on the annual cycle (Figure 6). The temporal relationship between the borehole water levels and the occurrence of the fracture swarms is consistent with a scenario where elevated fluid pressures reduced the effective stress and triggered fracture opening in critically stressed rock near the borehole walls (e.g., Ellsworth 2013).

### 3.2 Fracture Propagation Rates

Fractures in crustal rocks usually propagate at speeds approaching that of elastic waves (typically km/s (Scholz 2019)), which is about five orders of magnitude faster than the propagation speeds of ∼6 to 20 $cm.s^{-1}$ we observed. These propagation rates are similar to those observed for slow-slip events in other fault systems (Sacks et al. 1978; Kaproth and Marone 2013; Ikari et al. 2013; Uchida et al. 2016; Gualandi et al. 2020; Ide and Beroza 2023), which are often interpreted as modulated by the combined effects of fluid transport and attendant variations in pore fluid pressure (Segall et al. 2010; Brantut 2021; Ciardo and Lecampion 2019; Ozawa, Yang, and Dunham 2024). In this scenario, fracture propagation is limited by the time it takes for pressurized fluid to migrate into the newly opened fracture cavities. Using the hydraulic fracture model described in Figure 7, we estimate that the downward migration speed of fractures opening on the borehole wall should scale according to:

$$v_{c,z} \sim \frac{\rho_w g}{\mu_w}\left(\frac{K_{Ic}^2(1-\nu)}{\mathcal{G}T}\right)^2. \tag{7}$$

In the equation above, $\mu_w$ and $\rho_w$ characterize the pore fluid viscosity and density, $\mathcal{G}$, $\nu$ and $K_{I,c}$ describe the shear modulus, Poisson's ratio and tensile fracture toughness of the host rock, and $g$ is the gravitational acceleration. Assuming nominal values of $K_{Ic} = 2\text{MPa.m}^{1/2}$, $T = 5$ MPa, $\mathcal{G} = 20$ GPa, $\nu = 0.25$, $\rho_w = 1000$ kg.m$^{-3}$, and $\mu_w = 10^{-3}$ Pa.s yields a downward rupture speed on the order of a few cm.s$^{-1}$, in agreement with our observations. In addition, the model predicts that the rupture propagation speed should be independent of depth, which also agrees with our observations. We thus find that pore fluid processes likely played a role in both triggering the fracture swarms and modulating their propagation speed.

## 4 Conclusions

The hydrophone array data we acquired provides the first observations of fracturing in a peridotite borehole. The occurrence of the fracture swarms during a period of elevated pore pressure following large rain events more than two years after the borehole was established indicates that stress levels at the tip of the drilling-induced tensile fractures remained at near-critical levels over an extended period of time. These high stress levels allowed fracture swarms to be triggered by relatively small ($\sim$50 kPa) reductions in effective stress. The downward migrating fracture swarms exclusively begin in regions at the same depth interval where high pH and very low oxygen fugacity are found in recovered water samples, evidence of active, ongoing serpentinization. The correspondence of the depth interval of fracturing to the depth interval of active serpentinization suggests that water-rock reactions played a role in maintaining near-critical stresses at the crack tips, consistent with the reaction-driven fracturing hypothesis. The slow ($\sim$6 to 20 $cm \cdot s^{-1}$) propagation rates of the fracture swarms is consistent with pore fluid modulation of fracture propagation (i.e., dilatant hardening), similar to slow earthquakes and consistent with stress conditions near the stability threshold where small fluid pressure changes modulate fracture propagation rates (Segall et al. 2010).

Our results indicate that it may not be difficult to stimulate fracture growth for geological carbon sequestration efforts at the MBO site, or other sites like it. The slow propagation rates (6-20 cm/s) suggest that controlled pressure cycling during carbon dioxide injection could maximize fracture network development while avoiding excessive overpressure that might compromise seal integrity or lead to anthropogenic seismicity (Kelemen, Matter, Streit, et al. 2011). Serpentinization reactions can produce 2-4 kg $H_2/m^3$ of rock, and the demonstrated fracture enhancement could significantly increase reaction rates and hydrogen recovery motivating economic hydrogen production (Templeton, Ellison, Kelemen, et al. 2024).

## Open Research Section

Hydrophone data have been archived at the IRIS DMC (network code 7F 2019-2020, https://doi.org/10.7914/SN/7F_2019). The lithological data, borehole BA1D water level data, and televiewer data can be downloaded from the Inter-Continental Drilling Program data repository https://www.icdp-online.org/projects/by-continent/asia/oodp-oman/public-data-1. Precipitation data is available through the Copernicus data repository and Google Earth Engine https://code.earthengine.google.com/65cfcd01ee34290615a7c854a00b76f4. Please see supplemental python and matlab codes in the associated github repository: https://github.com/SerpRateAI/tensilePaper.

### Acknowledgments

This project received funding from the Norwegian Research Council (SerpRateAI, grant no. 334395), the European Research Council under the ERC Advanced Grant no. 101019628 "Break Through Rocks", and the US National Science Foundation (grant no. EAR-1516313). Greg Hirth acknowledges support from a Brown University SEED grant from the Initiative for Sustainable Energy. We thank Paul Fucile for his efforts to design and install the hydrophone arrays. John M. Aiken also would like to thank Varvara Bazilova who taught how to analyse ERA5-land and HydroBASINS data sets using Google Earth Engine and which was invaluable to this work. François Renard and Fabian Barras acknowledge support from the project FricFrac funded by the Center for Advanced Study (CAS) at the Norwegian Academy of Science and Letters during the academic year 2023-2024. The authors are grateful to Issa El-Hussain and Sultan Qaboos University for logistical assistance with the fieldwork. The authors thank the Ministry of Regional Municipalities and Water Resources in the Sultanate of Oman (particularly Eng. Sadi Al Habsi, Dr. Rashid Al Abri, Eng. Haider Ahmed Mohammed Alajmi, Ali Al Shukali Eng. Abduallah Al Kasbi, Said Al Mangi), and Eng. Zaher Al Sulaimani and Mazin Al Sulaimani from AZD Engineering for their logistical and technical support.

The authors have no conflicts of interest to declare.

## References

Aiken, John M., Elliot Dufornet, et al. (2025). "An AI-Enabled Data Processing Pipeline for Ingesting Borehole Data in Peridotite Environments". In: *Journal of Geophysical Research: Machine Learning and Computation* 2.2, e2025JH000666. DOI: https://doi.org/10.1029/2025JH000666.

Aiken, John M., Robert A. Sohn, et al. (2022). "Gas Migration Episodes Observed During Peridotite Alteration in the Samail Ophiolite, Oman". In: *Geophysical Research Letters* 49.21. e2022GL100395 2022GL100395, e2022GL100395. DOI: https://doi.org/10.1029/2022GL100395.

Brantut, Nicolas (Nov. 2021). "Dilatancy Toughening of Shear Cracks and Implications for Slow Rupture Propagation". In: *Journal of Geophysical Research: Solid Earth* 126.11. ISSN: 2169-9313, 2169-9356. DOI: 10.1029/2021JB022239.

Callegari, Ivan et al. (2022). "Tectonic transition from thrusting to polyphase non-confining deformation within the Semail Ophiolite along the sinistral, transtensional Issmaiya Fault Zone (Sultanate of Oman)". In: *Journal of Asian Earth Sciences* 224, p. 105007. ISSN: 1367-9120. DOI: https://doi.org/10.1016/j.jseaes.2021.105007.

Ciardo, F. and B. Lecampion (2019). "Effect of Dilatancy on the Transition From Aseismic to Seismic Slip Due to Fluid Injection in a Fault". In: *Journal of Geophysical Research: Solid Earth* 124.4, pp. 3724–3743. DOI: https://doi.org/10.1029/2018JB016636.

Cochard, T. et al. (2024). "Propagation of extended fractures by local nucleation and rapid transverse expansion of crack-front distortion". In: *Nature Physics* 20, pp. 660–665. DOI: https://doi.org/10.1038/s41567-023-02365-0.

Ellsworth, William L. (2013). "Injection-Induced Earthquakes". In: *Science* 341.6142, p. 1225942. DOI: 10.1126/science.1225942.

Gislason, Sigurdur R and Eric H. Oelkers (2014). "Carbon storage in basalt". In: *Science* 344.6182, pp. 373–374.

Gualandi, A. et al. (2020). "The predictable chaos of slow earthquakes". In: *Science Advances* 6.27, eaaz5548. DOI: 10.1126/sciadv.aaz5548.

Hatakeyama, Kohei et al. (2021). "Effects of Alteration and Cracks on the Seismic Velocity Structure of Oceanic Lithosphere Inferred From Ultrasonic Measurements of Mafic and Ultramafic Samples Collected by the Oman Drilling Project". In: *Journal of Geophysical Research: Solid Earth* 126.11, e2021JB021923. DOI: https://doi.org/10.1029/2021JB021923.

Ide, Satoshi and Gregory C Beroza (2023). "Slow earthquake scaling reconsidered as a boundary between distinct modes of rupture propagation". In: *Proceedings of the National Academy of Sciences* 120.32, e2222102120. DOI: https://doi.org/10.1073/pnas.2222102120.

Ikari, Matt J et al. (2013). "Slip weakening as a mechanism for slow earthquakes". In: *Nature geoscience* 6.6, pp. 468–472. DOI: https://doi.org/10.1038/ngeo1818.

Iyer, Kyle. et al. (2008). "Reaction-assisted hierarchical fracturing during serpentinization". In: *Earth and Planetary Science Letters* 267.3, pp. 503–516. ISSN: 0012-821X. DOI: https://doi.org/10.1016/j.epsl.2007.11.060.

Jaeger, John Conrad, Neville GW Cook, and Robert Zimmerman (2009). *Fundamentals of rock mechanics*. John Wiley & Sons. DOI: 10.1017/CBO9780511735349.

Jamtveit, Bjørn, Christine V Putnis, and Anders Malthe-Sørenssen (2009). "Reaction induced fracturing during replacement processes". In: *Contributions to Mineralogy and Petrology* 157.1, pp. 127–133. DOI: 10.1007/s00410-008-0324-y.

Kaproth, Bryan M. and C. Marone (2013). "Slow Earthquakes, Preseismic Velocity Changes, and the Origin of Slow Frictional Stick-Slip". In: *Science* 341.6151, pp. 1229–1232. DOI: 10.1126/science.1239577.

Katayama, Ikuo et al. (2020). "Permeability Profiles Across the Crust-Mantle Sections in the Oman Drilling Project Inferred From Dry and Wet Resistivity Data". In: *Journal of Geophysical Research: Solid Earth* 125.8, e2019JB018698. DOI: https://doi.org/10.1029/2019JB018698.

Kelemen, Peter B. and Greg Hirth (2012). "Reaction-driven cracking during retrograde metamorphism: Olivine hydration and carbonation". In: *Earth and Planetary Science Letters* 345-348, pp. 81–89. ISSN: 0012-821X. DOI: https://doi.org/10.1016/j.epsl.2012.06.018.

Kelemen, Peter B., James A. Leong, et al. (2021). "Initial Results From the Oman Drilling Project Multi-Borehole Observatory: Petrogenesis and Ongoing Alteration of Mantle Peridotite in the Weathering Horizon". In: *Journal of Geophysical Research: Solid Earth* 126.12, e2021JB022729. DOI: https://doi.org/10.1029/2021JB022729.

Kelemen, Peter B., J.M. Matter, D.A.H. Teagle, et al. (2020). "Scientific Drilling in the Samail Ophiolite, Sultanate of Oman". In: *Proceedings of the Oman Drilling Project*. DOI: 10.14379/Oman.ph1-2.proc.2020.

Kelemen, Peter B., Juerg M. Matter, Elisabeth E. Streit, et al. (2011). "Rates and Mechanisms of Mineral Carbonation in Peridotite: Natural Processes and Recipes for Enhanced, in situ CO2 Capture and Storage". In: *Annual Review of Earth and Planetary Sciences* 39.1, pp. 545–576. DOI: 10.1146/annurev-earth-092010-152509.

Kelemen, Peter B. and Jürg Matter (2008). "In situ carbonation of peridotite for CO¡sub¿2¡/sub¿ storage". In: *Proceedings of the National Academy of Sciences* 105.45, pp. 17295–17300. DOI: 10.1073/pnas.0805794105.

Lehner, Bernhard and Günther Grill (2013). "Global river hydrography and network routing: baseline data and new approaches to study the world's large river systems". In: *Hydrological Processes* 27.15, pp. 2171–2186. DOI: https://doi.org/10.1002/hyp.9740.

Liu, Tianze et al. (In Review). "Seismic Evidence for Sustained Gas Migration in a Serpentinizing Aquifer". In: *Geology*. URL: https://www.researchsquare.com/article/rs-7217354/v1.

Lods, Gérard et al. (2020). "Groundwater flow characterization of an ophiolitic hard-rock aquifer from cross-borehole multi-level hydraulic experiments". In: *Journal of Hydrology* 589, p. 125152. ISSN: 0022-1694. DOI: https://doi.org/10.1016/j.jhydrol.2020.125152.

Maeda, Naoki (1985). "A method for reading and checking phase times in autoprocessing system of seismic wave data". In: *Zisin* 38, pp. 365–379. DOI: https://doi.org/10.4294/zisin1948.38.3_365.

Malvoisin, Benjamin, Nicolas Brantut, and Mary-Alix Kaczmarek (2017). "Control of serpentinisation rate by reaction-induced cracking". In: *Earth and Planetary Science Letters* 476, pp. 143–152. ISSN: 0012-821X. DOI: https://doi.org/10.1016/j.epsl.2017.07.042. URL: https://www.sciencedirect.com/science/article/pii/S0012821X17304260.

Moore, J. Casey et al. (2011). "Growth of borehole breakouts with time after drilling: Implications for state of stress, NanTroSEIZE transect, SW Japan". In: *Geochemistry, Geophysics, Geosystems* 12.4. DOI: https://doi.org/10.1029/2010GC003417.

Okamoto, Atsushi and Hiroyuki Shimizu (2015). "Contrasting fracture patterns induced by volume-increasing and -decreasing reactions: Implications for the progress of metamorphic reactions". In: *Earth and Planetary Science Letters* 417, pp. 9–18. ISSN: 0012-821X. DOI: https://doi.org/10.1016/j.epsl.2015.02.015. URL: https://www.sciencedirect.com/science/article/pii/S0012821X1500093X.

Ozawa, So, Yuyun Yang, and Eric M. Dunham (2024). "Fault-Valve Instability: A Mechanism for Slow Slip Events". In: *Journal of Geophysical Research: Solid Earth* 129.10, e2024JB029165. DOI: https://doi.org/10.1029/2024JB029165.

Plümper, Oliver et al. (2012). "The interface-scale mechanism of reaction-induced fracturing during serpentinization". In: *Geology* 40.12, pp. 1103–1106. DOI: 10.1130/G33390.1.
Renard, François (2021). "Reaction-induced fracturing: When chemistry breaks rocks". In: *Journal of Geophysical Research: Solid Earth* 126.2, e2020JB021451.
Sacks, I Selwyn et al. (1978). "Slow earthquakes and stress redistribution". In: *Nature* 275.5681, pp. 599–602. DOI: https://doi.org/10.1038/275599a0.
Schoenberg, Michael et al. (Nov. 1981). "Space–time dependence of acoustic waves in a borehole". In: *The Journal of the Acoustical Society of America* 70.5, pp. 1496–1507. ISSN: 0001-4966. DOI: 10.1121/1.387107.
Scholz, Christopher H (2019). *The mechanics of earthquakes and faulting*. Cambridge university press.
Segall, Paul et al. (2010). "Dilatant strengthening as a mechanism for slow slip events". In: *Journal of Geophysical Research: Solid Earth* 115.B12. DOI: https://doi.org/10.1029/2010JB007449.
Sohn, R.A. and J.M. Matter (2023). "The response of borehole water levels in an ophiolitic, peridotite aquifer to atmospheric, solid Earth, and ocean tides". In: *Journal of Hydrology X* 21, p. 100163. ISSN: 2589-9155. DOI: https://doi.org/10.1016/j.hydroa.2023.100163.
Store, Copernicus Climate Change Service Climate Data (2017). *Copernicus Climate Change Service (C3S) (2017): ERA5: Fifth generation of ECMWF atmospheric reanalyses of the global climate*. Accessed 2024-01-25. DOI: 10.1002/qj.3803. URL: https://cds.climate.copernicus.eu/cdsapp#!/home.
Templeton, Alexis S., Eric T. Ellison, Clemens Glombitza, et al. (2021). "Accessing the Subsurface Biosphere Within Rocks Undergoing Active Low-Temperature Serpentinization in the Samail Ophiolite (Oman Drilling Project)". In: *Journal of Geophysical Research: Biogeosciences* 126.10. e2021JG006315 2021JG006315, e2021JG006315. DOI: https://doi.org/10.1029/2021JG006315.
Templeton, Alexis S., Eric T. Ellison, Peter B. Kelemen, et al. (2024). "Low-temperature hydrogen production and consumption in partially-hydrated peridotites in Oman: implications for stimulated geological hydrogen production". In: *Frontiers in Geochemistry* 2, p. 1366268. DOI: 10.3389/fgeoc.2024.1366268.
Uchida, Naoki et al. (2016). "Periodic slow slip triggers megathrust zone earthquakes in northeastern Japan". In: *Science* 351.6272, pp. 488–492. DOI: 10.1126/science.aad3108.
Zheng, Ziqiong, John Kemeny, and Neville G. W. Cook (1989). "Analysis of borehole breakouts". In: *Journal of Geophysical Research: Solid Earth* 94.B6, pp. 7171–7182. DOI: https://doi.org/10.1029/JB094iB06p07171.
Zoback, Mark D. et al. (1985). "Well bore breakouts and in situ stress". In: *Journal of Geophysical Research: Solid Earth* 90.B7, pp. 5523–5530. DOI: https://doi.org/10.1029/JB090iB07p05523.